RESEARCH ARTICLE

High-Performance Stretchable Supercapacitors Based on Centrifugal Electrospinning-Directed Hetero-structured Graphene–Polyaniline Hierarchical Fabric

Yun Zheng[1] · Zengming Man[1,2] · Yang Zhang[1,2] · Guan Wu[1,2] · Wangyang Lu[1,2] · Wenxing Chen[1,2]

Abstract

Stretchable supercapacitors (S-SCs) are of considerable interest as prospective energy-storage devices for wearable electronics and smart products. However, achieving high energy density and stable output under large deformations remains an urgent challenge. Here, we develop a high-performance S-SC based on a robust heterostructured graphene–polyaniline (G-PANI) anchored hierarchical fabric (G-PANI@pcPU). By precisely manipulating centrifugal electrospinning and PANI-induced two-step self-assembly process, the G-PANI@pcPU features an inter-linkage porous backbone, which open ions migration/intercalation pathways, high mechanical flexibility (elongation: 400%), and large production area (> 90 cm^2). The resultant G-PANI@pcPU presents ultra-large specific areal capacitance (C_{areal}) of 5093.7 mF cm^{-2} (about 35 mg cm^{-2} mass loading of G-PANI) and redox reversibility in 1 M H$_2$SO$_4$ electrolyte. Additionally, the G-PANI@pcPU fabric-based solid-state S-SCs show a high energy density of 69.2 μWh cm^{-2} and capacitance of 3113.7 mF cm^{-2}. More importantly, the superior stretchable stability (84.1% capacitance retentions after 5000 cycles) and foldable performance (86.7% capacitance retentions after 5000 cycles) of S-SCs are impressively achieved. Finally, the S-SCs realize potential applications of steady powering light-emitting diode (LED) lights at 100% strain, smart watch at bending deformation, toy car, and lamp. This work can offer an overwhelming foundation for designing advanced flexible electrodes toward new energy and smart wearable applications.

Keywords Stretchable supercapacitor · Hierarchical fabric · Deformable stability · Hetero-structured graphene–polyaniline · Wearable application

Introduction

With the advent of the 5G era, the Internet of Everything has become possible. Smart wearable textiles developed based on textile materials, which can sense and reply to environmental irritation from thermal, mechanical, electronic, chemical, and other aspects, are in an epoch of vigorous development [1–6]. These textiles endow ordinary textiles with new functions, including diagnosis, sensing, communication, navigation, and innovative fashion [7–9]. Continuous and stable energy is needed to support these new properties. Supercapacitors are promising energy-storage devices, because they can deliver excellent cycle life and high power densities and are among the most advanced energy-storage devices by far [10–13]. Furthermore, operational safety makes it highly competitive in many applications, such as biosensors [14, 15] and microelectronic devices [16, 17]. Nonetheless, how to power various electronics under large deformations by supercapacitors with high energy density remains an enormous challenge.

To guarantee the sustainable operation of the entire wearable electronic system, the relevantly flexible power device should output a steady and lasting electrical energy supply under various deformation situations, such as twisting, bending, and stretching [18–23]. However, off-the-shelf energy devices usually suffer from shortcomings, including large volume, heavy quality, high mechanical strength, and

✉ Guan Wu
gwu2016@zstu.edu.cn

✉ Wangyang Lu
luwy@zstu.edu.cn

[1] National Engineering Lab for Textile Fiber Materials and Processing Technology, Zhejiang Sci-Tech University, Hangzhou 310018, China

[2] Zhejiang Provincial Innovation Center of Advanced Textile Technology, Shaoxing 312000, China

low energy density, which cannot satisfy the requirements of wearable electronic systems [24]. Usually, the conventional preparation of supercapacitor electrodes is applied by mixing active materials with conductive agents and binders into a slurry, thereby coating them on current collectors (e.g., metal foil [25, 26] or carbon cloth [27, 28]). Such a procedure causes severe rigid, low energy density and less stretchability than conventional supercapacitors. Fabric- or fiber-based supercapacitors stand out for their high power density, rate capacity, and long-term cycling stability, along with their superior mechanical elongation, good knittability, and ease of integration [29, 30]. Noticeably, fabric- and fiber-based electrodes combined with elastic polymers (including polydimethylsiloxane (PDMS) [31, 32], Ecoflex [33], and polyurethane (PU) [34, 35]) will endow excellent tensile properties and tensile recoverability. For instance, Zhang et al. developed a stretchable supercapacitor composed of carbon nanotubes (CNTs) integrated in PDMS substrates, exhibiting a capacitance of 0.6 mF cm^{-2} under stretching from 0 to 200% [36]. Pullanchiyodan et al. fabricated supercapacitors using Ecoflex as the encapsulation material and MnO$_x$ as the pseudocapacitor, which showed a specific capacitance of 580 mF cm^{-2}, energy density of 51.4 μWh cm^{-2}, and capacitance retention above 90% upon 40% stretching for 1000 cycles [37]. In addition, Jeong et al. fabricated stretchable PU electrodes by spraying reduced graphene oxide (RGO)/single-walled carbon nanotube composites on gold-coated PU substrates. The maximum capacitance of the unstretched PU supercapacitor was 43 F g^{-1}, which decreased to 31 F g^{-1} after experiencing 100 cycles of stretching (72% retention) [38]. Impressively, the mechanical and electrochemical performances were enhanced by the abovementioned methods. However, the energy density of the electrodes decreases extremely under large deformation due to limitations in the construction of micro/nanostructures, selection of active materials, and preparation methods, which completely limits the practical application of fabric supercapacitors.

Generally, the energy density is closely related to the specific surface area (SSA), Faraday redox reaction, and electrical conductivity of the electrode materials [39]. Polyaniline (PANI) has attracted much attention among various electrode materials owing to its superior conductivity, high capacity, low cost, and fast and reversible doping/dedoping kinetics [40]. A combination of carbon-based materials can be used to further improve the stability of PANI [41]. For instance, RGO with remarkable electrical conductivity, outstanding electrical double-layer capacitance (EDLC), and excellent mechanical strength is incorporated. Due to the strong π–π stacking force between PANI and RGO, they can be self-assembled into heterostructured graphene–polyaniline (G-PANI) composites, alleviating the restacking of pure RGO [42]. Furthermore, owing to the limitations of

solubility and dispersion of PANI in most organic solvents, current PANI-based fibers prepared by electrospinning or wet spinning are fabricated with low mechanical strength, uneven dispersion, and poor electronic conductivity, causing supercapacitors to maintain high energy density under large deformations [43–45]. To date, due to the combination of centrifugal force and electrostatic force, centrifugal electrospinning has been produced as an important measure for preparing micro/nanofibers with various advantages, including uniform structure, controllable preparation, excellent molecular orientation, and large-scale production [46–48]. Consequently, if the centrifugal electrospinning technology and PANI-induced self-assembly process are combined to prepare electroactive conductive fabric, in principle, the high energy density and large stretchable energy supply of stretchable supercapacitors (S-SCs) will be realized. However, to the best of our knowledge, this strategy of fabricating supercapacitor electrodes remains unexplored, which motivates us to develop better electrochemical and mechanical performances.

Herein, we fabricate high-performance S-SCs based on heterostructured G-PANI hierarchical fabric (G-PANI@pcPU) electrodes. Generally, the centrifugal electrospinning fabrication of a large elastic PU fabric substrate endows G-PANI@pcPU with a high mechanical elongation at break of 400%. In addition, the PANI-induced two-step solution self-assembly reaction enables G-PANI to be efficiently bridged on the surface of composite PU (cPU) fabrics with PANI deposition, forming PANI@cPU (pcPU). The as-fabricated G-PANI@pcPU has a highly aligned 3D network, enhanced SSA/porosity, and fast interfacial charge transfer. Impressively, the G-PANI@pcPU fabric exhibits excellent electrochemical energy-storage performance with a high specific areal capacitance (C_{areal}) of 5,093.7 mF cm^{-2} (at 1 mA cm^{-2} in H$_2$SO$_4$ electrolyte approximately 2 cm^2 in area and 35 mg cm^{-2} in mass loading). Subsequently, the G-PANI@pcPU fabrics are assembled into flexible S-SCs, which present a high C_{areal} of 3113.7 mF cm^{-2} at 0.2 mA cm^{-2} and a high energy density of 69.2 μWh cm^{-2}. Specifically, after continuous stretching and folding processes for 5000 cycles, the constructed S-SCs can maintain high deformable stabilities with good capacitive retentions of 84.1 and 86.7%, respectively. Benefiting from their admirably electrochemical and mechanical performances, the S-SCs realize potential applications of steady powering light-emitting diode (LED) lights at 100% strain, smart watches at bending deformation, toy cars, and lamps. These highly deformable supercapacitors will become promising candidates as a supplement or substitute for flexible batteries in new-generation energy-storage fields.

Experimental Section

Materials

Aniline (ANI, 99%), ammonium persulfate (APS, AR), polyvinyl alcohol (PVA), and hexafluoroisopropanol (HFIP, 99.5%) were purchased from Shanghai Aladdin Biochemical Technology Co., Ltd. Polyurethane (PU, D4335) was purchased from Zhejiang Huafon TPU Co., Ltd. PANI was purchased from Shanghai Macklin Biochemical Technology Co., Ltd. Hydrochloric acid (HCl, AR) and sulfuric acid (H_2SO_4, AR) were purchased from Hangzhou Shuanghanlin Chemical Reagent Co., Ltd. All materials were not further processed.

Centrifugal Electrospinning of Composite Fabric

The spinning solution was prepared by dissolving PU (2 g) in HFIP (16 mL), at room temperature with magnetic stirring until the PU was completely dissolved. Subsequently, PANI (2 g) was introduced and stirred for 24 h to obtain a uniformly mixed spinning solution. The prepared solutions were injected into the four chambers of our homemade centrifugal electrospinning device. The needle was 27 gauge (27G). The sprayed fibers were received by a collector covered with aluminum foil. The receiving distance, applied voltage, and centrifugal speed were 10 cm, 12 kV, and 3500 r/min, respectively. The resulting composite textiles were termed cPU. The method used to prepare the pure PU fiber film was the same.

Deposition of PANI on cPU

The first self-assembly of polyaniline on PU occurred through in situ chemical polymerization. The aniline and fiber films were added to HCl aqueous solution (1 M, 2.5 mL) and soaked for 3 h. An additional HCl aqueous solution (1 M, 2.5 mL) containing APS was quickly added to the above solution and stirred for 30 s. The molar ratio of ANI to APS was 4:1. After 24 h of reaction, the fiber fabric was carefully washed several times with deionized water and dried completely at 60 °C. The resulting composite textiles were termed pcPU.

Synthesis of G-PANI@pcPU

The G-PANI composites were prepared by aniline reduction of GO, followed by secondary self-assembly between PANI of pcPU and G-PANI to prepare G-PANI@pcPU. Fiber films and a certain mass of GO were added to a 1 M HCl ethanol solution (5 mL) dissolved in aniline (0.1 mL). The mixture was reacted at 70 °C for 24 h. In this preparation process, the GO contents were 30 mg, 40 mg, and 50 mg. Therefore, the corresponding elastic fiber films were termed G-PANI-1@pcPU, G-PANI@pcPU, and G-PANI-2@pcPU. The corresponding heterostructured G-PANI composites were named G-PANI-1, G-PANI, and G-PANI-2.

Characterization

The structural morphologies of the resulting materials were obtained by SEM (Zeiss vltra55, Germany) and TEM (Talos F200S, Thermo Scientific, USA). XPS was collected on a K-Alpha (Thermo Scientific, USA). The FT-IR spectra were obtained using a Nicolet 5700 spectrometer (Thermo Scientific, USA). XRD data were determined on a D8 Discover (Bruker, USA). The water contact angle experimental results were obtained from JY-82.

Electrochemical Measurements

A CHI760E electrochemical workstation was utilized to test all electrochemical performances of the G-PANI@pcPU electrodes and G-PANI@pcPU integrated S-SCs. In the electrode examination, a G-PANI@pcPU electrode ($\approx 2\ cm^2$), Ag/AgCl, H_2SO_4 (1 M), and platinum foil were employed as the working electrode, reference electrode, electrolyte, and counter electrode, respectively. The C_{areal} of the electrode was calculated from the GCD curve based on Eq. 1 as follows:

$$C_{areal} = \frac{2i \int V \mathrm{d}t}{\Delta V^2}, \tag{1}$$

where C_{areal} (mF cm^{-2}), i (mA cm^{-2}), t (s), and ΔV (V) are the volumetric capacitance, discharge current density, discharge time, and voltage range, respectively.

Fabrication of G-PANI@pcPU Symmetrical S-SCs

First, CNTs (0.08 g) were added to deionized water (20 mL) and sonicated for 30 min. The surface of G-PANI@pcPU was covered with a layer of CNTs (~ 5 mg cm^{-2}) by vacuum filtration as the current collectors. In a typical procedure, the H_2SO_4-PVA gel was prepared by adding H_2SO_4 (6 g) to deionized water (60 mL) with stirring at 85 °C until clear. A layer of electrolyte gel was coated on the surface of the electrode after filtering a layer of multiwalled carbon nanotubes as a current collector. Finally, two identical electrodes were pressed together to make S-SC after putting at 25 °C to evaporate excess water. The C_{areal} of S-SCs was calculated by Eq. 2 as follows:

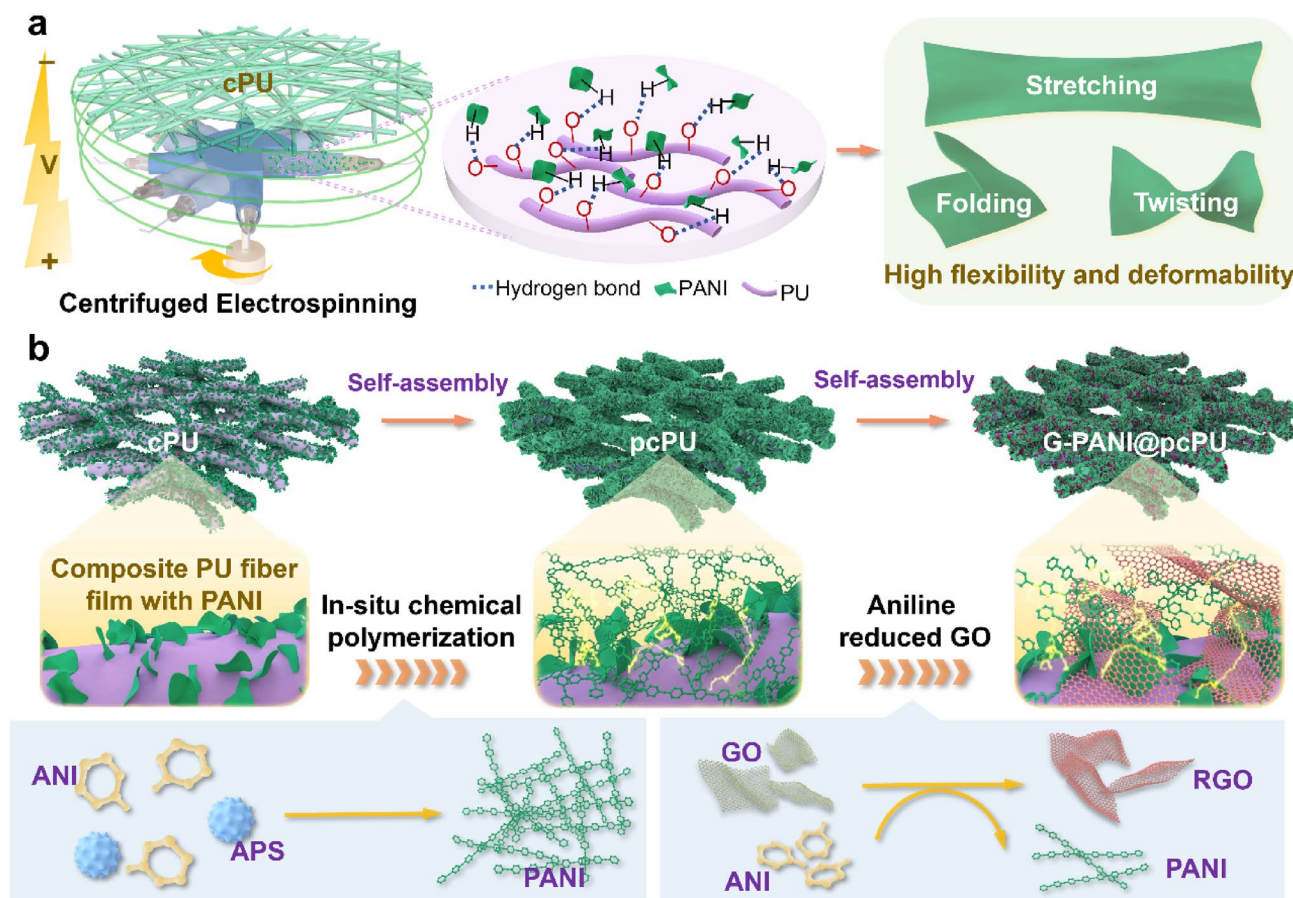$$C_{areal} = \frac{4 \times (2i \int V \mathrm{d}t)}{\Delta V^2}, \tag{2}$$

Fig. 1 Schematic illustration of the preparation of G-PANI@pcPU. **a** Centrifugal electrospinning fabrication of cPU fabric by the physical mixing of PU and PANI. **b** Two-step self-assembly fabrication of G-PANI@pcPU: in situ polymerization of PANI on cPU fabric and further aniline-induced reduction of GO

where C_{areal} (mF cm^{-2}), i (mA cm^{-2}), t (s), and ΔV (V) are the volumetric capacitance, discharge current density, discharge time, and voltage range, respectively.

The energy density (E, μWh cm^{-2}) and power density (P, μW cm^{-2}) were calculated according to Eqs. 3 and 4, respectively

$$E = \frac{C_{\text{areal}} \times \Delta V^2}{8 \times 3.6}, \tag{3}$$

$$P = \frac{E \times 3600}{\Delta t}. \tag{4}$$

Results and Discussion

Figure 1 illustrates the fabrication process of the G-PANI@pcPU fabric electrode. Typically, a desired dispersion of polyurethane and PANI solution was spun into composite PU (cPU) fabrics with excellent flexibility and deformability

(Fig. 1a). In this stage, the strong hydrogen bond between PU and PANI increases the miscibility and mixing uniformity of the PANI chain and PU matrix [49, 50], thereby generating plentiful active sites for the subsequent PANI-induced self-assembly reaction. Then, the G-PANI@pcPU fabric was gradually constructed by immersing the cPU fabric into aniline and aniline and graphene oxide (GO) solutions, respectively, undergoing two self-assembly reactions (Fig. 1b). In the first step, the surface of cPU is chemically polymerized with a large loading of PANI, which is defined as PANI@cPU (pcPU). In the second step, G-PANI was deposited on the pcPU surface to form the G-PANI@pcPU fabric, which is beneficial for increasing the capacity. In this stage, aniline could reduce GO and simultaneously undergo oxidative polymerization to produce heterostructured G-PANI composites (Fig. S1) [51]. Additionally, we explored the electrochemical performance of the G-PANI@pcPU fabric by regulating the different proportions of aniline and GO. The prepared fabrics were termed G-PANI-1@pcPU (30 mg GO), G-PANI@pcPU (40 mg GO), and G-PANI-2@pcPU (50 mg GO). The corresponding heterostructured G-PANI
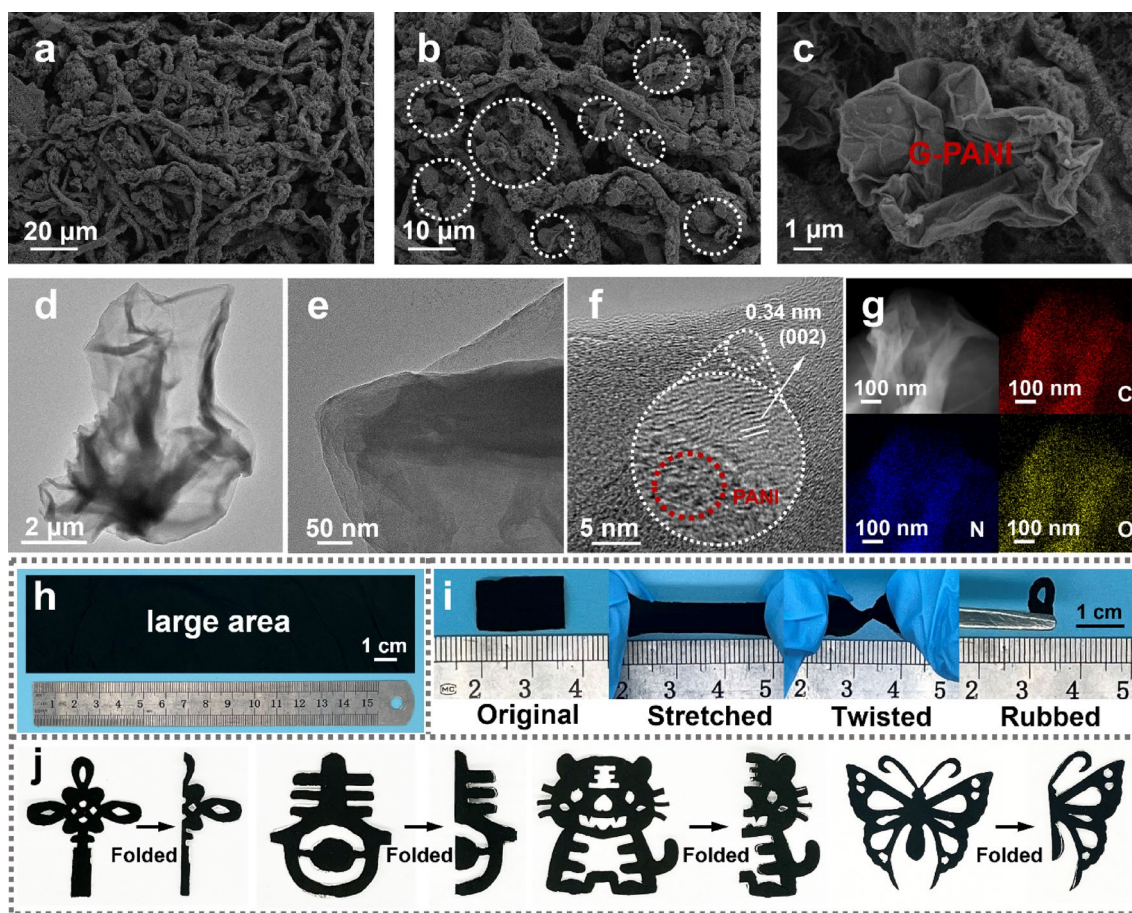
Fig. 2 **a-c** SEM images of G-PANI@pcPU. **d-f** TEM images of G-PANI. **g** EDS mapping for C, N, and O elements of G-PANI. **h** Photograph of large-scale preparation. **i** Photographs of G-PANI@ pcPU under different deformations. **j** Photographs of G-PANI@pcPU cropped into different shapes under folding/unfolding states

composites were named G-PANI-1, G-PANI, and G-PANI-2. Satisfyingly, centrifugal electrospinning and two self-assembly reaction processes endow the heterostructured G-PANI hierarchical fabrics with many advantages. (1) Through centrifugal electrospinning, uniform PANI-dispersed compact fibers were produced at a large scale (> 90 cm^2), with excellent mechanical stability, high flexibility (elongation: 400%), sufficiently guaranteeing the high deformable stability of S-SCs for driving wearable electronics under continuous stretching operation. (2) The two self-assembly reactions between PANI and RGO enable G-PANI composites to be efficiently bridged on the surface of cPU fabrics, verifying a highly aligned 3D network, developed SSA/porosity, and fast interfacial charge transfer, which can facilitate electrolyte ions with kinetic diffusion and accessible intercalation. (3) The high areal capacitance, energy density, and stretchable energy supply performances of S-SCs, along with practical applications for steady powering of LED lights at high strain, smart watches at bending deformation, toy cars, and lamps, have proven to show significant potential in future

new energy and textile systems toward smart and flexible wearable applications.

We used scanning electron microscopy (SEM) and transmission electron microscopy (TEM) to evaluate the microstructural morphologies of the G-PANI@pcPU fabrics and G-PANI composites, respectively. Compared with the morphologies of cPU (Fig. S2a, b), pcPU has more PANI layers covering the fabric after polymerization (Fig. S2c, d). Additionally, after two self-assembly process treatments, G-PANI@pcPU presents the densest PANI deposition with an obvious G-PANI connection, forming a good electron transport network (Fig. 2a, b). As seen in the high magnification images in Fig. 2c, the crumpled morphology of G-PANI can offer a large accessible surface for electrolyte ion adsorption. TEM images (Fig. 2d, e, f) were used to further ascertain the wrinkled structure of G-PANI. At a higher magnification (Fig. 2f inset), a lattice fringe of 0.34 nm is observed, which is in accordance with natural graphite [52]. Clearly, GO is successfully reduced to RGO by aniline [53]. Furthermore, the formation of
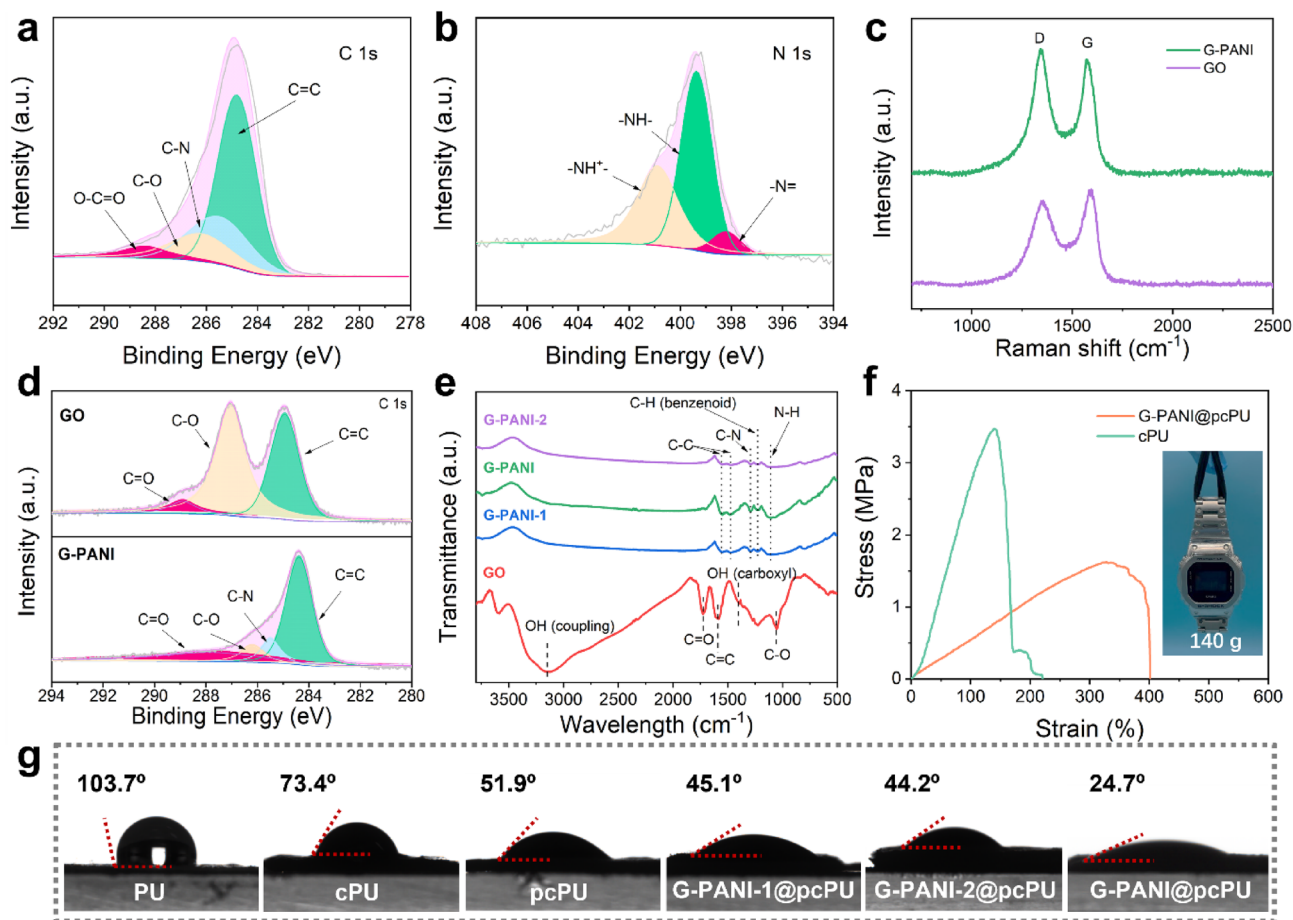
Fig. 3 **a** C 1 s and **b** N 1 s XPS spectra of the G-PANI@pcPU fabric. **c** Raman spectra, **d** C 1 s XPS spectra of GO and G-PANI. **e** FT-IR spectra of GO and different G-PANI composites. **f** Mechanical prop-erties of the cPU and G-PANI@pcPU fabrics. Inset: photograph of G-PANI@pcPU fabric suspending a weight of 140 g. **g** The water contact angles of various fabrics

PANI on the RGO surface can guarantee a good redox reaction. The spatial distributions of elements are explored by EDS mapping (Fig. 2g). The uniform distributions of N, C, and O elements also indicate the good deposition of PANI on the RGO surface. Based on this extensible centrifugal electrospinning fabrication, G-PANI@pcPU fabrics can be produced in large areas exceeding 90 cm^2 (Fig. 2h). In addition, due to the excellent flexibility and stretchability of the PU substrate, the G-PANI@pcPU fabrics can withstand various large deformations, such as stretching, twisting, rubbing, and folding (Fig. 2i). Simul-taneously, the G-PANI@pcPU fabrics exhibit robust pro-cessability and can be tailored into different shapes, which can satisfactorily fulfill the requirements of practical appli-cations toward wearable electronics (Fig. 2j).

X-ray photoelectron spectroscopy (XPS) analysis was further executed to examine the characteristic binding energies of the C 1 s and N 1 s peaks of the G-PANI@pcPU fabrics. In Fig. S3, the peaks located at 284.8, 400.6, and 532.9 eV can be allocated to C 1 s, N 1 s, and O 1 s,

respectively, which further confirm the presence of C, N, and O in G-PANI@pcPU [54]. As shown in Fig. 3a, the C1s peak is composed of four Gaussian peaks with binding ener-gies of C=C (284.8 eV), C–N (285.5 eV), C–O (286.2 eV), and O–C=O (288.4 eV). The existence of the C–N peak composition at 285.5 eV demonstrates that a considerable amount of PANI is compounded with RGO [55]. The N 1 s spectrum in Fig. 3b indicates that most N atoms of PANI are in the form of benzenoid amine (–NH–) centralized at 399.4 eV with secondary small peaks, including quinoid imine (–N=) (398.2 eV) and positively charged N atoms (–NH$^+$–) (401.0 eV) [51]. Figure S4 shows the X-ray dif-fraction (XRD) curves. For pure PU, the diffraction peak appeared at approximately $2\theta = 20°$, indicating the crystal-linity of polyurethane [56]. Compared with pure PU, cPU shows obvious characteristic peaks of PANI. The character-istic peaks of PANI emerge at $2\theta = 15.1°$, 20.9°, and 25.1° on the broad background. The peaks at 25.1° and 20.9° are the crystalline peak and amorphous peak, respectively [57]. The characteristic peaks of the G-PANI@pcPU fabric are

similar to those of cPU. Moreover, the crystalline peak at 25.1° is sharper than that of cPU, which implies an increase in the crystalline phase and strengthened stacking along the specific direction of PANI in the G-PANI@pcPU fabric [58]. This is possibly due to aniline polymerization on the surfaces of RGO, wherein the confined spaces can induce alignment in PANI chains and lead to higher crystallinity [59].

Raman spectra were used to demonstrate that GO was successfully reduced by aniline. As shown in Fig. 3c, the D and G band peaks appear at ∼ 1330 and ∼ 1600 cm^{-1}, respectively. Generally, the I_D/I_G ratio increases from 0.85 to 1.14, indicating that the reduction of GO did take place. In addition, the C 1 s XPS spectrum (Fig. 3d) was employed to analyze GO and G-PANI. Although G-PANI and GO show the same oxygen functional group, the peak intensity of G-PANI is much smaller than that of GO, proving considerable deoxygenation by the reduction process. The reduction of GO by aniline is also confirmed by Fourier transform-infrared spectroscopy (FT-IR). As described in Fig. 3e, the C=O-stretching vibration peak (1726 cm^{-1}), the vibration and deformation peaks of O–H groups (3395 cm^{-1} and 1410 cm^{-1}), and the C–O-stretching peak (1052 cm^{-1}) decrease dramatically or disappear. These observations confirm that most of the oxygen functional groups in GO are removed. We further used FT-IR spectroscopy to investigate the effect of different GO contents on the formation of G-PANI. Typically, all resultant G-PANI composites possess the characteristic peaks of PANI, such as C–C stretching of the quinonoid ring and benzenoid ring at 1561 and 1466 cm^{-1}, C–N stretching of secondary aromatic amines at 1299 cm^{-1}, C–H stretching of the benzenoid ring at 1244 cm^{-1}, and –NH– bond at 1140 cm^{-1} ascribed to the emeraldine form of PANI [60, 61]. It has been reported that the –NH– bond determines the conductivity of PANI in different oxidation states. Impressively, G-PANI maintains a higher absorption peak intensity than G-PANI-1 and G-PANI-2, implying the best electrochemical performance [57].

The mechanical properties of the cPU and G-PANI@ pcPU fabrics were investigated by stress−strain measurements (Fig. 3f). The G-PANI@pcPU fabric is found to provide a tensile strength of 1.61 MPa with a large elongation at break of 400%. Compared with cPU, G-PANI@pcPU exhibits distinctly improved tensile stain, which is attributed to the incorporation of RGO. The decrease in tensile strength may result from the PU structure being destroyed by the acidic environment during the reaction [62]. Astonishingly, the G-PANI@pcPU fabric can easily bear a weight of 140 g (Fig. 3f inset). Water droplet contact angle measurements are executed to determine the interaction between the electrode liquid/solid interface. After a two-step self-assembly treatment, the average contact angles on the G-PANI@pcPU electrode surfaces drop sharply compared with that of cPU. The G-PANI@pcPU electrode has the smallest water contact angle (24.7°), confirming sufficient infiltration of the electrolyte. Notably, the hydrophilic surface of the electrodes is crucial to obtain better performance, because it facilitates fast ion diffusion and accumulation [63].

The electrochemical characteristics of the cPU, pcPU, G-PANI-1@pcPU, G-PANI-2@pcPU, and G-PANI@pcPU electrodes were investigated using a three-electrode system in a 1 M H$_2$SO$_4$ electrolyte. Figure 4a demonstrates that the G-PANI@pcPU electrode exhibits the largest cyclic voltammetry (CV) curve area compared to those of cPU and pcPU (Figs. S5, 6, 7) after two self-assembly reactions. Moreover, the energy-storage capacities of different G-PANI@pcPU fabrics were evaluated by controlling the GO content in the second self-assembly process. The results showed that the CV area of G-PANI@pcPU (40 mg GO) was larger than that of G-PANI-1@pcPU (30 mg GO, Fig. S8) and G-PANI-2@ pcPU (50 mg GO, Fig. S9). A larger CV area leads to better charge storage and electrochemical performance. Impressively, the CV curves show rectangular shapes with superimposed redox peaks, indicating the coexistence of electric double-layer capacitance and pseudocapacitance. However, the CV curves are distorted at high scan rates due to the pseudoreversible kinetics of PANI redox [64]. The galvanostatic charge/discharge (GCD) curves (Figs. 4b, S10, 11, 12, 13, 14) reveal that G-PANI@pcPU possesses the best energy-storage capability and invertible ion transportation. Figure 4c shows the specific areal capacitance derived from the GCD curves. Significantly, G-PANI@pcPU shows the highest capacitance (1512.5 mF cm^{-2} at 2 mA cm^{-2}), which is much better than those of cPU (39.5 mF cm^{-2}), pcPU (101 mF cm^{-2}), G-PANI-1@pcPU (560.8 mF cm^{-2}), and G-PANI-2@pcPU (1114.4 mF cm^{-2}).

Figures 4d and S15 depict the Nyquist plots simulated by the equivalent circuit model, featuring a depressed semicircle (high frequencies), Warburg diffusion (medium frequencies), and vertical line of intercalation capacitance (low frequencies). In this system, the internal resistance (R_0), charge transfer resistance/double-layer capacitance (C_1/R_1), diffusion impedance (Z_w), and intercalation capacitance (C_2) were utilized. As obtained from the simulated results in Table S1, pcPU maintains a lower R_0 of 3.03 Ω compared to cPU (4.21 Ω), which is due to the enhancement of conductivity by the chemical polymerization of PANI. After anchoring G-PANI, the internal resistance of G-PANI@ pcPU further decreases to 1.87 Ω. In addition, G-PANI@ pcPU maintains the lowest C$_1$/R$_1$ resistance of 1.87 Ω/0.67 mF compared to cPU (22.5 Ω/0.16 mF) and pcPU (14.3 Ω/0.24 mF). It was found that G-PANI further increases the electrical conductivity and double-layer capacitance. The Z_w, G-PANI@pcPU has a smallest resistance (4.8 Ω) compared to those of cPU (153.9 Ω) and pcPU (36.5 Ω), revealing that G-PANI introduces abundant porous channels for electrolyte ion fast dynamic diffusion. Therefore, G-PANI@pcPU has
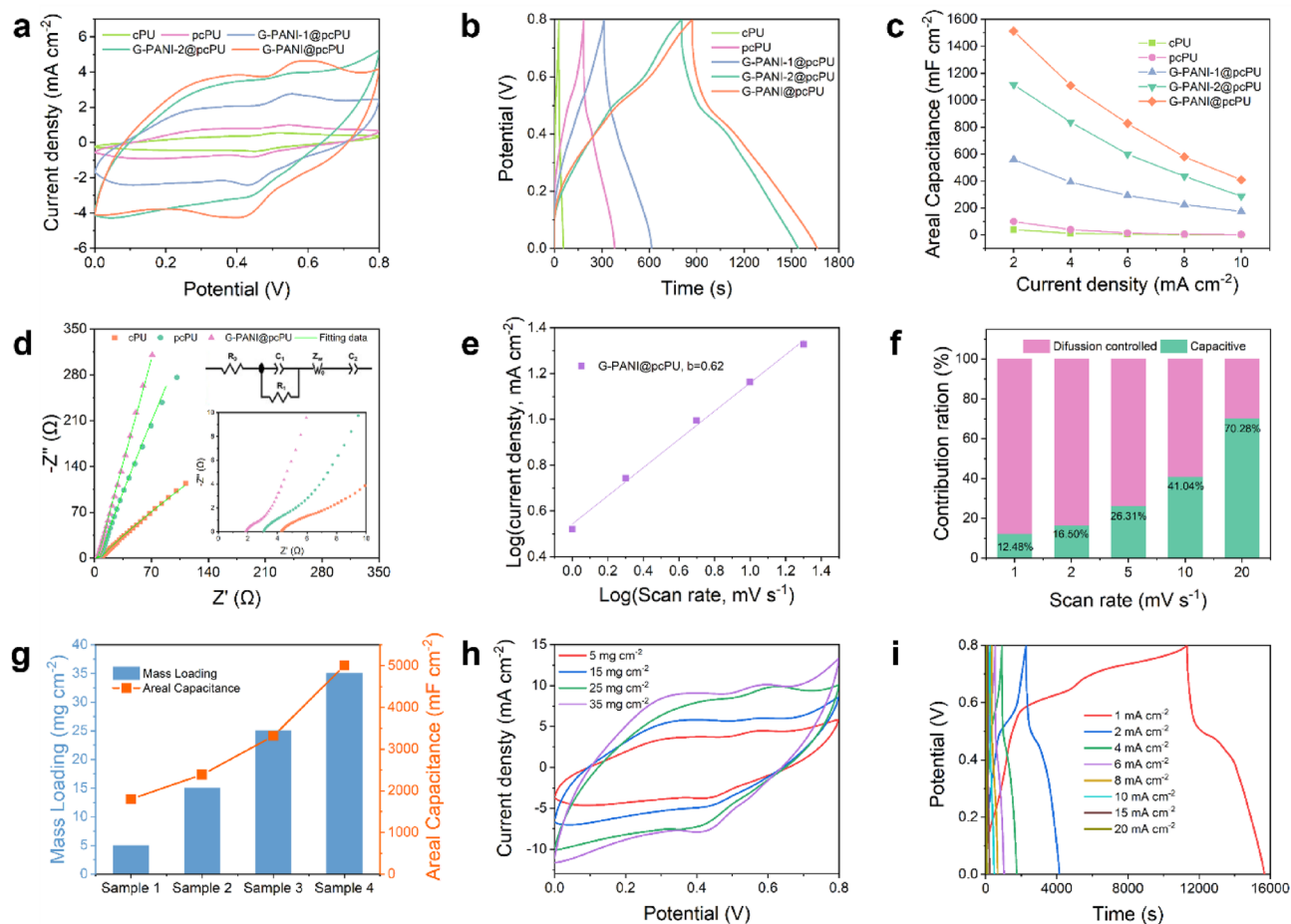
Fig. 4 Electrochemical performances of electrodes in a 1 M H_2SO_4 electrolyte. **a** CV curves at 2 mV s^{-1}. **b** GCD curves at 2 mA cm^{-2}. **c** Specific areal capacitances at different current densities and **d** EIS of cPU, pcPU, G-PANI-1@pcPU, G-PANI-2@pcPU, and G-PANI@pcPU. Inset: the depressed semicircle and equivalent circuit model of

Nyquist plots. **e** Log (scan rate) versus log (peak current) graph of the G-PANI@pcPU fabric. **f** Capacitive contributions at different scan rates. **g** Specific areal capacitances and **h** CV curves at different mass loading of G-PANI@pcPU. **i** Specific areal capacitances at different current densities of G-PANI@pcPU when the load is 35 mg cm^{-2}

a higher intercalation capacitance (12.6 mF) compared to those of cPU (0.83 mF) and pcPU (1.5 mF). As described in Fig. S16, compared to pcPU, G-PANI@pcPU contains more meso- and macropores. The resultant G-PANI@pcPU exhibits an SSA of 19.43 m^2 g^{-1}, which is larger than that of pcPU (5.06 m^2 g^{-1}) and can provide smooth pathways for ion accumulating and transporting. Electrochemical kinetic analysis was further performed to investigate the energy-storage mechanism controlled by the electrode surface capacitance and diffusion of the G-PANI@pcPU electrode. The current I is related to the scan rate following the equation $I_p = av^b$ [65], where I_p, v, a, and b are the peak current, scan rate, and constant terms, respectively (Fig. 4e). After calculation, the b value is 0.62 by fitting the peak currents at 1 to 20 mV s^{-1}, indicating that the electrochemical behavior of G-PANI@pcPU involves diffusion and capacitive control processes [66]. Moreover, the detailed capacitive contributions at different scan rates are shown in Figs. S17 and 4f.

When the scan rate increases, an increasing trend in capacitance control and a decreasing trend in diffusion contribution are observed. Typically, the capacitive contribution reaches up to 70.3% at a high scan rate of 20 mV s^{-1}.

In addition, the energy-storage performances under different load masses were also explored. When the loading mass of G-PANI on pcPU was controlled at 35 mg cm^{-2}, the C_{areal} of the G-PANI@pcPU fabric reached up to 5093.7 mF cm^{-2} (Fig. 4g). Figures 4h and S7, 18, 19, 20 exhibit the CV curves of the G-PANI@pcPU electrode under different mass loadings. When the load was 35 mg cm^{-2}, it also presented the largest CV curve area. The specific areal capacitances calculated from the GCD curves (Figs. 4i, S21, 22, 23) show that a good C_{areal} can be retained at 455 mF cm^{-2} at a higher current density of 20 mA cm^{-2}.

To further enrich the practical applications, a solid-state symmetric flexible S-SC is constructed by assembling two G-PANI@pcPU fabric electrodes with one conductive

H_2SO_4-polyvinyl alcohol (H_2SO_4-PVA) electrolyte layer. Figure 5a shows that no obvious redox peaks are inspected in the CV curves of symmetric G-PANI@pcPU S-SC, which is due to the overlapping of redox transformation processes of PANI between the leucoemeraldine and pernigraniline states. The GCD curves of G-PANI@pcPU S-SC in the range of 0.2 to 2 mA cm^{-2} show an asymmetric triangle shape and some initial potential drops, which is ascribed to the high resistance of the insulating elastic PU substrate. In addition, Fig. 5c shows the C_{areal} of G-PANI@pcPU S-SC by GCD curve calculation. The highest C_{areal} of the device is 3,113.7 mF cm^{-2} at 0.2 mA cm^{-2}, which retains a good capacitance of 615.5 mF cm^{-2} at 2 mA cm^{-2}. More meaningful parameters, including energy density and power density, are used for evaluation. As described from the Ragone plot (Fig. 5d), G-PANI@pcPU S-SC has high energy densities of 69.2–13.7 μWh cm^{-2} at power densities of 41.9–263.0 μW cm^{-2}. To the best of our knowledge, this level is superior to that of most stretchable supercapacitors reported in the literature (CNT/PEDOT:PSS of 3.6 μWh cm^{-2}; Ag-O$_x$-SWCNT of 0.41 μWh cm^{-2}; Mo@Paper of 4 μWh cm^{-2}; PANI@F-MWCNT@silk of 12.2 μWh cm^{-2}; CNT/MnO$_2$ of 15.2 μWh cm^{-2}; anodized Mo of 0.37 μWh cm^{-2}; MXene@CW of 10.1 μWh cm^{-2}; 3D porous PEDOT:PSS/graphene of 2.24 μWh cm^{-2}) [67–74].

Long-term cycling stability was measured to estimate the cycle life of G-PANI@pcPU S-SC, as shown in Fig. 5e. A capacitance retention of 86.7%, along with a coulombic efficiency of 96.7%, at 2 mA cm^{-2} after 8000 cycles is realized for G-PANI@pcPU S-SC, demonstrating good cycling stability. By connecting two G-PANI@pcPU S-SCs in series (Fig. 5f), the output voltage can be increased from 0.8 to 1.6 V at a current density of 2 mA cm^{-2}. Obviously, the output current can be increased by paralleling two G-PANI@pcPU S-SCs, wherein the discharge time is approximately two times larger, compared with that of a single S-SC under the same operating voltage. To satisfy the essential wearable applications, the deformable stability of the device was also evaluated. As shown in Fig. 5g, the CV curves of S-SC basically show no notable changes under different folded angles from 0 to 180°. Additionally, when the S-SC is repeatedly applied in the 120° folded state for 5000 cycles, an excellent capacitance retention of 86.7% is obtained. The S-SC also maintains remarkable stretchable stability when withstanding 20 to 80% stretched deformations. Furthermore, the S-SC preserves a significant capacitance retention of 84.1% when suffering from the 60% strain of consecutive stretching. Notably, these high folding/stretchable performances result from centrifugal electrospinning and two-step self-assembly processes, which are vital for smart electronics and wearable devices. The efficient energy-storage mechanism is illustrated in Fig. 5i. Due to the incoherent conductive network of cPU fibers, only minimal pseudocapacitance can be generated from redox reactions, and fewer ions can be accessed by electrolyte ions for slow migration and infiltration. After *in situ* polymerization of PANI and introduction of G-PANI, the extended conductive networks on PU fibers are coherently constructed, which promotes interlayer electron conduction, making it highly interfacial charge transfer and reversible charge/discharge capability.

Our efforts have been focused on developing substantial application archetypes with potentially practical uses. Generally, as demonstrated in Fig. 6a and Video S1, the S-SC significantly lights up the integration of 3 LEDs in parallel. The stretching of S-SC has no noticeable impact on the brightness of the LEDs from 30 to 100% stretched deformations, making it suitable for applications in smart wearable electronics. As shown in Figs. S24, S25, Video S2, and Video S3, the above conclusion can also be drawn when S-SC in other deformation (such as twisted and rubbed) lights up LED. Despite being stretched at 50% deformation, the S-SC can reliably power the calculator (Fig. S26). Afterward, it can be applied to provide an energy supply for real-life objects, such as a watch (Figs. 6b, S27 and Video S4). Impressively, finger joint movement does not have a considerable influence on the performance of the power supply. The S-SC can offer sufficient energy supply to drive an electric fan (Fig. S28) as well as a toy car (Fig. 6c, Video S5). It can provide enough energy for a toy car to move forward approximately 70 cm. To verify its application under high-power needs, three S-SCs were connected in series to light lamps with greater power (Fig. 6d, Video S6). By efficiently powering those useful devices, G-PANI@pcPU S-SC demonstrates great potential as a supplement or replacement for flexible batteries in the future.

Conclusions

In summary, we report a heterostructured G-PANI hierarchical fabric. Centrifugal electrospinning and solution self-assembly resulted in uniform G-PANI@pcPU structure, with outstanding elasticity (elongation: 400%), large-scale production (> 90 cm^2), and superior C_{areal} (5093.7 mF cm^{-2} in H_2SO_4 electrolyte). The solid-state super capacitor (S-SC) made of this electrospun G-PANI@pcPU delivers a high areal energy density of 69.2 μWh cm^{-2}, capacitance of 3113.7 mF cm^{-2}, and sustainable performance versus stretching (84.1% capacitance retention after 5000 cycles), and folding (86.7% capacitance retention after 5000 cycles), in the H_2SO_4-PVA electrolyte. Notably,
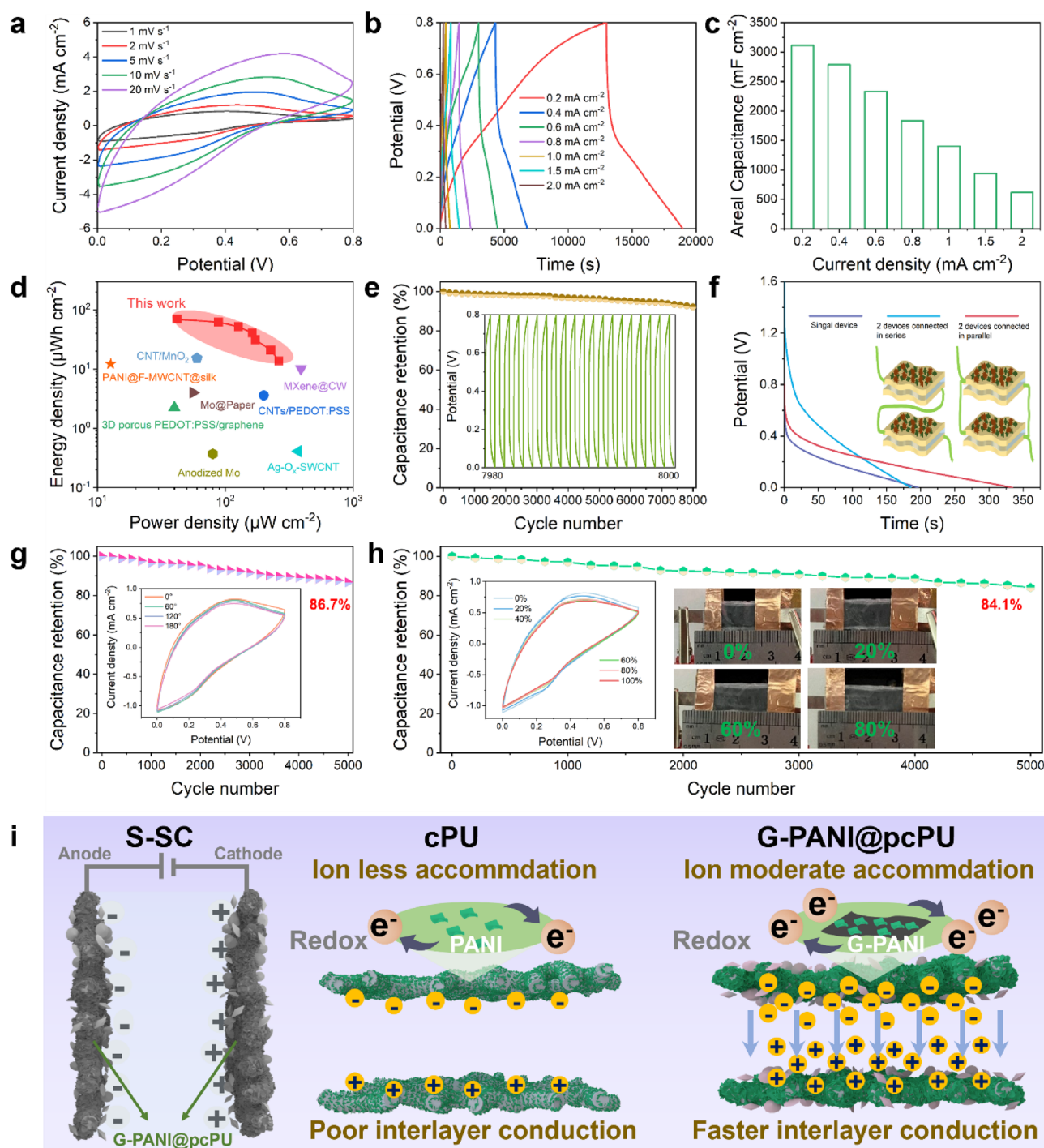
Fig. 5 Electrochemical performances of symmetric G-PANI@pcPU S-SC. **a** CV curves at different scan rates. **b** GCD curves at different current densities. **c** C_{areal} under different current densities. **d** Power densities vs energy densities and their comparisons. **e** Cycling stability at 2 mA cm^{-2}. Inset: GCD curves for the last 20 cycles. **f** GCD curves of single S-SC, two S-SC connected in series and parallel at the current density of 2 mA cm^{-2}. **g** Folding stability. Inset: CV curves of different folding angles at 2 mV s^{-1}. **h** Tensile stability. Inset: CV curves and photographs of S-SCs under different stretch strains at 2 mV s^{-1}. **i** Schematic mechanism for high energy-storage performances of S-SCs
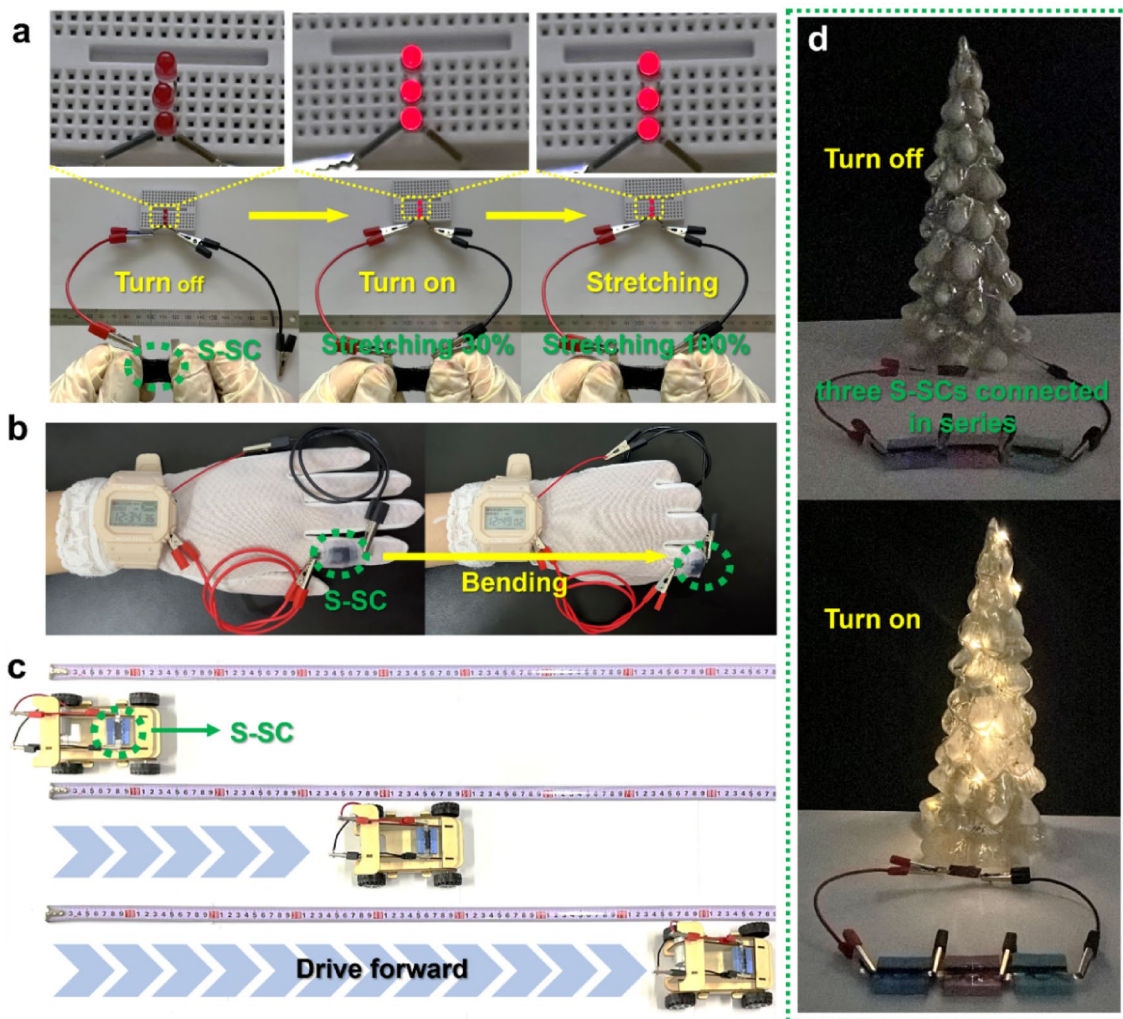
Fig. 6 The prototypes of actual powered applications. **a** Photographs of S-SC to power LEDs under stretching states. **b** Photographs of S-SC to power watch under bending states. **c** Photographs of S-SC to power toy car. **d** Photographs of three S-SC in series to power lamp

the G-PANI@pPU S-SCs can power LED lights at 100% strain, smart watches at bending deformation, toy cars, and lamps. Our work offers a significant step to realize the advanced electrode design and manufacturing of flexible supercapacitors in energy-storage technology, which might provide a new idea to guide development in the wearable industry.

Data availability The authors declare that the data supporting the findings of this study are available within the paper and its Supplementary Information files. Should any raw data files be needed in another format they are available from the corresponding author upon reasonable request. Source data are provided with this paper.

Declarations

Conflict of Interest The authors declare that they have no known competing financial interests or personal relationships that could have influenced the work reported in this paper.

References

1. Rogers JA, Someya T, Huang YG. Materials and mechanics for stretchable electronics. *Science*. **2010**;*327*:1603.

2. Pomerantseva E, Bonaccorso F, Feng XL, Cui Y, Gogotsi Y. Energy storage: the future enabled by nanomaterials. *Science*. **2019**;*366*:969.

3. Liu CL, Bai Y, Li WT, Yang FY, Zhang GX, Pang H. In situ growth of three-dimensional MXene/metal-organic framework composites for high-performance supercapacitors. *Angew Chem Int Edit*. **2022**;*61*: e202116282.

4. Zhou Z, Li P, Man Z, Zhu X, Ye S, Lu W, Wu G, Chen W. Multiscale dot-wire-sheet heterostructured nitrogen-doped carbon dots-$Ti_3C_2T_x$/silk nanofibers for high-performance fiber-shaped supercapacitors. *Angew Chem Int Edit*. **2023**. https://doi.org/10.1002/anie.202301618.

5. Li M, Li Z, Qu L, Chen F, Tian M. Recent progress of the active materials with various micro-structures for flexible textile-based supercapacitors. *Adv Fiber Mater*. **2022**;*4*:1005.

6. Niu L, Wang J, Wang K, Pan H, Jiang G, Chen C, Ma P. High-speed sirospun conductive yarn for stretchable embedded knitted circuit and self-powered wearable device. *Adv Fiber Mater*. **2022**;*5*:154.

7. Li ZN, Gadipelli S, Li HC, Howard CA, Brett DJL, Shearing PR, Guo ZX, Parkin IP, Li F. Tuning the interlayer spacing of graphene laminate films for efficient pore utilization towards compact capacitive energy storage. *Nat Energy*. **2020**;*5*:345.

8. Yi P, Zou H, Yu Y, Li X, Li Z, Deng G, Chen C, Fang M, He J, Sun X, Liu X, Shui J, Yu R. MXene-reinforced liquid metal/polymer fibers via interface engineering for wearable multifunctional textiles. *ACS Nano*. **2022**;*16*:14490.

9. Mun TJ, Kim SH, Park JW, Moon JH, Jang Y, Huynh C, Baughman RH, Kim SJ. Wearable energy generating and storing textile based on carbon nanotube yarns. *Adv Funct Mater*. **2020**;*30*:2000411.

10. Farahani FS, Rahmanifar MS, Noori A, El-Kady MF, Hassani N, Neek-Amal M, Kaner RB, Mousavi MF. Trilayer metal-organic frameworks as multifunctional electrocatalysts for energy conversion and storage applications. *J Am Chem Soc*. **2022**;*144*:15903.

11. Lee J, Zambrano BL, Woo J, Yoon K, Lee T. Recent advances in 1D stretchable electrodes and devices for textile and wearable electronics: materials, fabrications, and applications. *Adv Mater*. **2020**;*32*:1902532.

12. Yu CY, An JN, Chen Q, Zhou JY, Huang W, Kim YJ, Sun GZ. Recent advances in design of flexible electrodes for miniaturized supercapacitors. *Small Methods*. **2020**;*4*:1900824.

13. Yu Y, Pan D, Zhao L, Huang S, Lin P, Wang Z, Jia Y, Wang H, Wang L. Paper-like polyphenylene sulfide/aramid fiber electrode with excellent areal capacitance and flame-retardant performance. *Adv Fiber Mater*. **2022**;*4*:1246.

14. Ray TR, Choi J, Bandodkar AJ, Krishnan S, Gutruf P, Tian LM, Ghaffari R, Rogers JA. Bio-Integrated wearable systems: a comprehensive review. *Chem Rev*. **2019**;*119*:5461.

15. Park H, Kim JW, Hong SY, Lee G, Lee H, Song C, Keum K, Jeong YR, Jin SW, Kim DS, Ha JS. Dynamically stretchable supercapacitor for powering an integrated biosensor in an all-in-One textile system. *ACS Nano*. **2019**;*13*:10469.

16. Keum K, Kim JW, Hong SY, Son JG, Lee SS, Ha JS. Flexible/stretchable supercapacitors with novel functionality for wearable electronics. *Adv Mater*. **2020**;*32*:2002180.

17. Karnaushenko D, Kong T, Bandari VK, Zhu F, Schmidt OG. 3D self-assembled microelectronic devices: concepts, materials, applications. *Adv Mater*. **2020**;*32*:1902994.

18. Wu TY, Wu XJ, Li LH, Hao MM, Wu G, Zhang T, Chen S. Anisotropic boron-carbon hetero-nanosheets for ultrahigh energy density supercapacitors. *Angew Chem Int Edit*. **2020**;*59*:23800.

19. Atta MM, Fahim RA. Flexible and wearable supercapacitors: a short review. *J Energy Storage*. **2021**;*44*: 103475.

20. Dong L, Xu C, Li Y, Huang Z-H, Kang F, Yang Q-H, Zhao X. Flexible electrodes and supercapacitors for wearable energy storage: a review by category. *J Mater Chem A*. **2016**;*4*:4659.

21. Jia R, Shen GZ, Qu FY, Chen D. Flexible on-chip micro-supercapacitors: efficient power units for wearable electronics. *Energy Storage Mater*. **2020**;*27*:169.

22. Cheng HY, Meng JK, Wu G, Chen S. Hierarchical micro-mesoporous carbon-framework-based hybrid nanofibres for high-density capacitive energy storage. *Angew Chem Int Edit*. **2019**;*58*:17465.

23. Xue Q, Sun J, Huang Y, Zhu M, Pei Z, Li H, Wang Y, Li N, Zhang H, Zhi C. Recent progress on flexible and wearable supercapacitors. *Small*. **2017**;*13*:1701827.

24. Wu TY, Ma ZY, He YY, Wu XJ, Tang B, Yu ZY, Wu G, Chen S, Bao NZ. A covalent black phosphorus/metal-organic framework hetero-nanostructure for high-performance flexible supercapacitors. *Angew Chem Int Edit*. **2021**;*60*:10366.

25. Yang XW, Lin ZX, Zheng JX, Huang YJ, Chen B, Mai YY, Feng XL. Facile template-free synthesis of vertically aligned polypyrrole nanosheets on nickel foams for flexible all-solid-state asymmetric supercapacitors. *Nanoscale*. **2016**;*8*:8650.

26. Yu JH, Wu JF, Wang HZ, Zhou A, Huang CQ, Bai H, Li L. Metallic fabrics as the current collector for high-performance graphene-based flexible solid-state supercapacitor. *ACS Appl Mater Inter*. **2016**;*8*:4724.

27. Miao ZY, Huang Y, Xin JP, Su XW, Sang YH, Liu H, Wang JJ. High-performance symmetric supercapacitor constructed using carbon cloth boosted by engineering oxygen-containing functional groups. *ACS Appl Mater Inter*. **2019**;*11*:18044.

28. Luo WS, Chen WC, Quan HY, Zhang ZX, Zeng Y, Wang YY, Chen DZ. Strongly coupled carbon quantum dots/NiCo-LDHs nanosheets on carbon cloth as electrode for high performance flexible supercapacitors. *Appl Surf Sci*. **2022**;*591*: 153161.

29. Guan T, Li Z, Qiu D, Wu G, Wu J, Zhu L, Zhu M, Bao N. Recent progress of graphene fiber/fabric supercapacitors: from building block architecture, fiber assembly, and fabric construction to wearable applications. *Adv Fiber Mater*. **2023**. https://doi.org/10.1007/s42765-023-00262-y.

30. Ramasubramanian B, Reddy VS, Zhen Y, Ramakrishna S, Chellappan V. Metal organic framework derived zirconia–carbon nanoporous mat for integrated strain sensor powered by solid-state supercapacitor. *Adv Fiber Mater*. **2023**. https://doi.org/10.1007/s42765-023-00283-7.

31. Song Y, Chen HT, Su ZM, Chen XX, Miao LM, Zhang JX, Cheng XL, Zhang HX. Highly compressible integrated supercapacitor-piezoresistance-sensor system with CNT-PDMS sponge for health monitoring. *Small*. **2017**;*13*:1702091.

32. Mao YY, Li Y, Xie JY, Liu H, Guo CJ, Hu WBA. Triboelectric nanogenerator/supercapacitor in-one self-powered textile based on PTFE yarn wrapped PDMS/MnO_2NW hybrid elastomer. *Nano Energy*. **2021**;*84*: 105918.

33. Yun J, Lim Y, Jang GN, Kim D, Lee SJ, Park H, Hong SY, Lee G, Zi G, Ha JS. Stretchable patterned graphene gas sensor driven by integrated micro-supercapacitor array. *Nano Energy*. **2016**;*19*:401.

34. Li TQ, Fang X, Pang Q, Huang WM, Sun JQ. Healable and shape editable supercapacitors based on shape memory polyurethanes. *J Mater Chem A*. **2019**;*7*:17456.

35. Li XY, Bandyopadhyay P, Kshetri T, Kim NH, Lee JH. Novel hydroxylated boron nitride functionalized p-phenylenediamine-grafted graphene: an excellent filler for enhancing the barrier properties of polyurethane. *J Mater Chem A*. **2018**;*6*:21501.

36. Zhang RZ, Ding JJ, Liu C, Yang EH. Highly stretchable supercapacitors enabled by interwoven CNTs partially embedded in PDMS. *ACS Appl Energ Mater*. **2018**;*1*:2048.

37. Pullanchiyodan A, Manjakkal L, Ntagios M, Dahiya R. MnO$_x$-electrodeposited fabric-based stretchable supercapacitors with intrinsic strain sensing. *ACS Appl Mater Inter*. **2021**;*13*:47581.

38. Jeong HT, Du JF, Kim YR, Raj CJ, Kim BC. Electrochemical performances of highly stretchable polyurethane (PU) supercapacitors based on nanocarbon materials composites. *J Alloy Compd*. **2019**;*777*:59.

39. Baker CO, Huang XW, Nelson W, Kaner RB. Polyaniline nanofibers: broadening applications for conducting polymers. *Chem Soc Rev*. **2017**;*46*:1510.

40. Dong LB, Liang GM, Xu CJ, Liu WB, Pan ZZ, Zhou EL, Kang FY, Yang QH. Multi hierarchical construction-induced superior capacitive performances of flexible electrodes for wearable energy storage. *Nano Energy*. **2017**;*34*:242.

41. Wu D, Yu CY, Zhong WB. Bioinspired strengthening and toughening of carbon nanotube@polyaniline/graphene film using electroactive biomass as glue for flexible supercapacitors with high rate performance and volumetric capacitance, and low-temperature tolerance. *J Mater Chem A*. **2021**;*9*:18356.

42. Hu RF, Zhao J, Zhu GD, Zheng JP. Fabrication of flexible free-standing reduced graphene oxide/polyaniline nanocomposite film for all-solid-state flexible supercapacitor. *Electrochim Acta*. **2018**;*261*:151.

43. Sukitpaneenit P, Thanpitcha T, Sirivat A, Weder C, Rujiravanit R. Electrical conductivity and mechanical properties of polyaniline/natural rubber composite fibers. *J Appl Polym Sci*. **2007**;*106*:4038.

44. Meng S, Zhang YY, Wu NH, Peng C, Huang ZY, Lin ZJ, Qi C, Liu Z, Kong TT. Ultrasoft, sensitive fiber-like sensor by assembly of bacterial cellulose (BC) nanofibrils and BC molecules for biocompatible strain sensing. *Nano Res*. **2022**;*16*:4067.

45. Liu WC, Chang YC, Zhang JW, Liu H. Wet-spun side-by-side electrically conductive composite fibers. *ACS Appl Electron Mater*. **1979**;*2022*:4.

46. Edmondson D, Cooper A, Jana S, Wood D, Zhang MQ. Centrifugal electrospinning of highly aligned polymer nanofibers over a large area. *J Mater Chem*. **2012**;*22*:18646.

47. Chang WM, Wang CC, Chen CY. Fabrication of ultra-thin carbon nanofibers by centrifuged-electrospinning for application in high-rate supercapacitors. *Electrochim Acta*. **2019**;*296*:268.

48. Valipouri A, Ravandi SAH, Pishevar AR. A novel method for manufacturing nanofibers. *Fiber Polym*. **2013**;*14*:941.

49. Feng JY, Shi H, Yang XY, Xiao S. Self-adhesion conductive sub-micron fiber cardiac patch from shape memory polymers to promote electrical signal transduction function. *ACS Appl Mater Inter*. **2021**;*13*:19593.

50. Fang YL, Xu JH, Gao F, Du XS, Du ZL, Cheng X, Wang HB. Self-healable and recyclable polyurethane-polyaniline hydrogel toward flexible strain sensor. *Compos Part B-Eng*. **2021**;*219*:108965.

51. Xu LQ, Liu YL, Neoh KG, Kang ET, Fu GD. Reduction of graphene oxide by aniline with its concomitant oxidative polymerization. *Macromol Rapid Comm*. **2011**;*32*:684.

52. Hou DD, Liu QF, Cheng HF, Li K, Wang D, Zhang H. Chrysanthemum extract assisted green reduction of graphene oxide. *Mater Chem Phys*. **2016**;*183*:76.

53. Lesiak B, Trykowski G, Toth J, Biniak S, Kover L, Rangam N, Stobinski L, Malolepszy A. Chemical and structural properties of reduced graphene oxide-dependence on the reducing agent. *J Mater Sci*. **2021**;*56*:3738.

54. Yu PP, Zhao X, Huang ZL, Li YZ, Zhang QH. Free-standing three-dimensional graphene and polyaniline nanowire arrays hybrid foams for high-performance flexible and lightweight supercapacitors. *J Mater Chem A*. **2014**;*2*:14413.

55. Zhang LL, Huang D, Hu NT, Yang C, Li M, Wei H, Yang Z, Su YJ, Zhang YF. Three-dimensional structures of graphene/polyaniline hybrid films constructed by steamed water for high-performance supercapacitors. *J Power Sources*. **2017**;*342*:1.

56. Zhang T, Xi K, Yu X, Gu M, Guo S, Gu B, Wang HZ. Synthesis, properties of fullerene-containing polyurethane–urea and its optical limiting absorption. *Polymer*. **2003**;*44*:2647.

57. Chaudhari HK, Kelkar DS. Investigation of structure and electrical conductivity in doped polyaniline. *Polym Int*. **1997**;*42*:380.

58. Kim M, Lee C, Jang J. Fabrication of highly flexible, scalable, and highperformance supercapacitors using polyaniline/reduced graphene oxide film with enhanced electrical conductivity and crystallinity. *Adv Funct Mater*. **2014**;*24*:2489.

59. Chen NL, Ren YP, Kong PP, Tan L, Feng HX, Luo YC. In situ one-pot preparation of reduced graphene oxide/polyaniline composite for high-performance electrochemical capacitors. *Appl Surf Sci*. **2017**;*392*:71.

60. Fei JB, Cui Y, Yan XH, Yang Y, Wang KW, Li JB. Controlled fabrication of polyaniline spherical and cubic shells with hierarchical nanostructures. *ACS Nano*. **2009**;*3*:3714.

61. Pan LJ, Pu L, Shi Y, Song SY, Xu Z, Zhang R, Zheng YD. Synthesis of polyaniline nanotubes with a reactive template of manganese oxide. *Adv Mater*. **2007**;*19*:461.

62. Krasowska K, Janik H, Gradys A, Rutkowska M. Degradation of polyurethanes in compost under natural conditions. *J Appl Polym Sci*. **2012**;*125*:4252.

63. Navale YH, Navale ST, Chougule MA, Ingole SM, Stadler FJ, Mane RS, Naushad M, Patil VB. Electrochemical synthesis and potential electrochemical energy storage performance of nodule-type polyaniline. *J Colloid Interf Sci*. **2017**;*487*:458.

64. Wu JF, Zhang QE, Wang JJ, Huang XP, Bai H. A self-assembly route to porous polyaniline/reduced graphene oxide composite materials with molecular-level uniformity for high-performance supercapacitors. *Energ Environ Sci*. **2018**;*11*:1280.

65. Wang YG, Song YF, Xia YY. Electrochemical capacitors: mechanism, materials, systems, characterization and applications. *Chem Soc Rev*. **2016**;*45*:5925.

66. Fleischmann S, Mitchell JB, Wang RC, Zhan C, Jiang DE, Presser V, Augustyn V. Pseudocapacitance: from fundamental understanding to high power energy storage materials. *Chem Rev*. **2020**;*120*:6738.

67. Yang JY, Cao QH, Tang XW, Du JJ, Yu T, Xu X, Cai DM, Guan C, Huang W. 3D-Printed highly stretchable conducting polymer electrodes for flexible supercapacitors. *J Mater Chem A*. **2021**;*9*:19649.

68. Lee H, Lee G, Yun J, Keum K, Hong SY, Song C, Kim JW, Lee JH, Oh SY, Kim DS, Kim MS, Ha JS. Facile fabrication of a fully biodegradable and stretchable serpentine-shaped wire supercapacitor. *Chem Eng J*. **2019**;*366*:62.

69. Yang HJ, Lee JW, Seo SH, Jeong B, Lee BH, Do WJ, Kim JH, Cho JY, Jo A, Jeong HJ, Jeong SY, Kim GH, Lee GW, Shin YE, Ko H, Han JT, Park JH. Fully stretchable self-charging power unit with micro-supercapacitor and triboelectric nanogenerator based

on oxidized single-walled carbon nanotube/polymer electrodes. *Nano Energy*. **2021**;*86*: 106083.

70. Wang ZF, Li X, Yang ZJ, Guo HC, Tan YJ, Susanto GJ, Cheng W, Yang WD, Tee BCK. Fully transient stretchable fruit-based battery as safe and environmentally friendly power source for wearable electronics. *Ecomat*. **2021**;*3*: e12073.

71. Zheng XH, Zhou XS, Xu J, Zou LH, Nie WQ, Hu XH, Dai SP, Qiu YP, Yuan NY. Highly stretchable CNT/MnO$_2$ nanosheets fiber supercapacitors with high energy density. *J Mater Sci*. **2020**;*55*:8251.

72. Zeng J, Dong LB, Sha WX, Wei L, Guo X. Highly stretchable, compressible and arbitrarily deformable all-hydrogel soft supercapacitors. *Chem Eng J*. **2020**;*383*: 123098.

73. Wang RY, Li WJ, Jiang L, Liu Q, Wang L, Tang B, Yang WY. Rationally designed hierarchical SiC@PANI core/shell nanowire arrays: toward high-performance supercapacitors with high-rate performance and robust stability. *Electrochim Acta*. **2022**;*406*: 139867.

74. Song P, Tao J, He XM, Sun YM, Shen XP, Zhai LZ, Yuan AH, Zhang DY, Ji ZY, Li BL. Silk-inspired stretchable fiber-shaped supercapacitors with ultrahigh volumetric capacitance and energy density for wearable electronics. *Chem Eng J*. **2020**;*386*: 124024.

Yun Zheng is currently pursuing a PhD at Zhejiang Sci-Tech University. Her research interests include materials science and textile technology, with a focus on the research of flexible supercapacitors.

Zengming Man received his Bachelor's degree graduated from Zhejiang Sci-Tech University in 2017, and received his PhD from the Nanjing University of Aeronautics and Astronautics in 2021. He joined the School of Materials Science and Engineering at Zhejiang Sci-Tech University in 2021. He mainly engages in research work in the field of new energy materials and devices.

Yang Zhang obtained his PhD from Donghua University in 2022 and later joined the School of Materials Science and Engineering at Zhejiang Sci-Tech University. His research mainly focuses on the construction of carbon-based hybrid fibers by wet spinning and the assembly of flexible energy storage devices.

Dr. Guan Wu received his Ph.D. in physical chemistry at Suzhou Institute of Nano-tech and Nanobionics, Chinese Academy of Sciences in 2016. He worked as a lecturer and associate professor at the State Key Laboratory of Material-Oriented Chemical Engineering, College of Chemical Engineering at Nanjing Tech University from 2016 to 2021. He is now a full professor at the School of Materials Science and Engineering, Zhejiang Sci-Tech University. His research interests include 2D nanomaterials, micro/nanofibers, supercapacitors, batteries, actuators, sensors, microfluidics and wearable devices.

Dr. Wangyang Lu is a distinguished full professor at Zhejiang Sci-Tech University. He has published over 70 papers and got over 30 issued patents. His research interests include catalytic functional fibers, functional polymer materials, and smart textiles.

Dr. Wenxing Chen is an academician of the CAE Member and a full professor of Zhejiang Sci-Tech University. He obtained a Ph.D. in Science from Zhejiang University in 1999 and a Ph.D. in Engineering from Shinshu University in Japan in 2000. His research activity focuses on polyester reaction engineering, research on environmental catalytic fibers, and research on intelligent fiber materials.